



DYE SENSITIZED SOLAR CELL (DSC) BASED ON REDUCED GRAPHENE OXIDE (rGO)-TiO₂ NANOCOMPOSITE PHOTOELECTRODE AND POLYANILINE (PANI) COUNTER ELECTRODE

Ahmed T.O.^{1*}, Ogunleye O.O.¹, Abdulrahaman A.Y.¹, Alu N.²

¹Department of Physics, Federal University Lokoja, P.M.B. 1154, Nigeria

²Physics Advanced Research Centre, Sheda Science and Technology Complex, Abuja, Nigeria

ARTICLE INFO

TYPE: Research Article

Received: 31/8/2020

Revised: 22/9/2020

Accepted: 23/9/2020

Published online: 30/9/2020

<https://doi.org/10.47869/tcsj.71.7.5>

*Corresponding author

Email: tajahmol@yahoo.co.uk; tajudeen.ahmed@fulokoja.edu.ng

Abstract. We report the successful application of reduced graphene oxide–titania (rGO–TiO₂) nanocomposite as an efficient photoelectrode and an inexpensive polyaniline (PANI) synthesized by in-situ polymerization on graphite foam as a platinum substitute for tri-iodide reduction for dye-sensitized solar cell (DSC). The bulk carrier concentration and conductivity of the PANI was measured to be $3.02 \times 10^{17} \text{ cm}^{-3}$ and $4.89 \times 10^{-1} \Omega^{-1} \text{ cm}^{-1}$ respectively. Subsequently, three DSCs were assembled with rGO–TiO₂ nanocomposite photoelectrode and PANI as counter electrode for one and the other two assembled using unmodified TiO₂ photoelectrode with PANI and platinum as counter electrodes, respectively. The rGO loading allows more dye to be adsorbed due its large surface area thus improving the light harvesting efficiency (LHE). This improvement in LHE increases the short circuit current density (J_{SC}). The J_{SC} increase is more substantial compared to the reduction in V_{OC} ; thus, the increase in the efficiency of the cell with rGO-TiO₂ nanocomposite electrode. The short circuit current density for the rGO-TiO₂ DSC with PANI counter electrode is 0.45 mA cm^{-2} while that for the unmodified TiO₂ DSCs with PANI counter electrode and platinum counter electrode are 0.11 mA cm^{-2} and 0.10 mA cm^{-2} respectively. This corresponds to 76% increase in the current density and it increases collection rate at the photoelectrode leading to enhanced power conversion efficiency of 0.13% compared with 0.04% and 0.02% for the DSCs assembled with unmodified TiO₂ under full sunlight illumination (100 mW/cm^2 , AM 1.5G) as a result of the better charge collection efficiency of rGO, which reduces the back electron transfer process. This represent 69% enhancement of energy conversion efficiency in the DSC consisting of rGO modified TiO₂.

Keywords: Dye sensitized solar cells, rGO-TiO₂ nanocomposite, PANI counter electrode,

1. INTRODUCTION

The salient features of a Dye-sensitized Solar Cell (DSC) include photoelectrode, photosensitizer, electrolyte, and counter electrode. The most significant of these is the photoelectrode that is fabricated using a nanoporous wide bandgap TiO_2 thin film. Another striking feature of the thin film photoelectrode is its enormous internal surface area that favors increased dye loading, light absorption, and interpenetration of liquid electrolyte [1]. A major limitation associated with the nanoporous photoelectrode is the non-uniform interfaces which create many trapping points (i.e., boundaries and defects) for electrons and consequently this leads to a decrease in the output current and power conversion efficiency [2]. Another challenge recognized to be a bottleneck for achieving higher power conversion in DSCs is the competition between the generation and recombination of photo-excited carriers [3]. However, research efforts made so far to ameliorate these challenges include the use of one-dimensional nanostructures to pave way for rapid collection of photo-generated electrons so as to reduce the rate of recombination and deposition of light scatterers onto TiO_2 photoelectrode surface in order to increase the light-harvesting capability of the photoelectrode. Much as good as these approaches, the drawbacks associated with them eventually limit the power conversion efficiency and increase the recombination rate of photo-generated carriers [1-3]. The inevitable high recombination rate associated with the use of modified TiO_2 photoelectrode is believed to emanate from the smallness of the particles which cannot form band bending [4-6]. This implies that an electric field that spatially separates the injected electrons from the holes in the dye or solution is not formed at the large electrode-electrolyte interface thus leading to high recombination currents [4-7]. This loss mechanism was overcome on one hand, by forming an insulating layer at the exposed TiO_2 photoelectrode surface [8-12]. On the other hand, by fabricating on the TiO_2 photoelectrode surface, an energy barrier that allows electron injection but stops the recombination reaction could be achieved [13-21]. One of such efforts is the formation of Nb_2O_5 on TiO_2 photoelectrode surface as an energy barrier and an enhancement in the performance of the fabricated DSC was achieved. Subsequently, when SrTiO_3 was coated on TiO_2 photoelectrode, an upward shift in the conduction band of TiO_2 led to a more significant increase in the open circuit voltage (V_{OC}) compared to the loss in the short circuit current density (J_{SC}) giving an overall increase in the cell efficiency [22-25].

Graphene is one of the most popular nanostructured materials with a two-dimensional honeycomb lattice structure consisting of a carbon six membered [26]. In recent years, graphene has been used as an efficient photocatalyst to improve the efficiency of an artificial photosynthesis system [27, 28]. Graphene oxide (GO) is one of the important derivatives of graphene and a new type of carbon material with excellent performance, high surface area and the rich functional groups on the surface gives its insulating ability [29, 30]. Reduced graphene oxide (rGO) that is highly conducting with improved electron mobility and charge capacity can be obtained by reducing GO [31, 32]. Consequently, when the surface oxygen-

containing functional groups of rGO is combined with semiconductor materials, rich binding sites results for enhanced photocatalytic performance [33-37]. Based on these reports, it is generally believed that this combination would lead to enhanced adsorption properties and the formation of carbon material/semiconductor interfaces to promote electron hole pair separation. Consequently, research efforts on DSCs using rGO-TiO₂ by [38, 39] led to enhanced dye adsorption properties with lower internal resistances, faster electron transport, lower charge recombination rate and a high current density. This was attributed to better charge collection efficiency of rGO, which reduced the back-electron transfer process [38].

In this paper, we report the synthesis of rGO-TiO₂ nanocomposite electrode and its effect on the performance of DSCs. The nanocomposite rGO-TiO₂ photoelectrode was examined by means of current-voltage (I-V) characteristics of the solar cell when illuminated and in the dark. The results indicate that, unlike the Nb₂O₅ that forms an energy barrier at the surface and SrTiO₃ that shifts the conduction band of the TiO₂ in the negative direction, rGO doping allows more dye to be adsorbed due its large surface area thus improving the light harvesting efficiency (LHE). This improvement in LHE increases the short circuit current density (J_{SC}). The J_{SC} increase is more significant compared to the reduction in V_{OC}; thus, the overall efficiency of the cell increased by 69% because TiO₂ core was decorated with rGO.

2. Materials and Methods

Titanium isopropoxide, Titanium nanoxide, reduced graphene oxide (rGO), acetylacetonate, ethanol, isopropanol, fluorine doped tin-oxide (FTO) conducting glass [11.40 ohm/m², (1.00 × 1.00) cm²], electrolyte (iodolyte-AN-50), sealing gasket (surlyn-SX1170-25PF), aniline, K₂Cr₂O₇ catalyst and vitriol (H₂SO₄) were all obtained from SOLARONIX. The as-received rGO was synthesized using modified Hummer's method. Dye extract was obtained from the natural product (*Delonix regia*). A mixture of 0.3M of titanium isopropoxide, 1.2M acetylacetonate and isopropanol was sequentially spin coated three (3) times with different concentrations as blocking layer on the pre-cleaned fluorine doped tin-oxide (FTO) conducting glasses and sintered at 150°C for four minutes each time the deposition was made. Subsequently, a paste of titanium nanoxide in propanol in the ratio 1:3 was screen printed on the three (3) fluorine doped tin-oxide (FTO) conducting glasses and allowed to dry at 125 °C in open air for 6 mins. Sequel to this, 10mg/ml of rGO was mixed with 70% acetone and 30% water and the mixture was deposited on FTO/TiO₂ glass electrodes. The rGO-TiO₂ photoelectrodes were annealed in a furnace at 300 °C for 40 mins and allowed to cool to room temperature to melt together the rGO-TiO₂ nanoparticles and to ensure good mechanical cohesion on the glass surface. Fresh leaves of *Delonix regia* were crushed into tiny bits and boiled in 75 ml of deionized water for 15 mins. The residue was removed by filtration and the resulting extract was centrifuged to further remove any solid residue. The dye extract was used directly as prepared for the construction of the DSCs at room temperature. A scattering layer of TiO₂ was also deposited on the TiO₂ electrodes before the electrodes were immersed (face-up) in the natural dye extract for complete sensitizer uptake at room temperature for 18 hrs. This turned the TiO₂ film from pale white to sensitizer colour. The excess dye was washed away with anhydrous ethanol and dried in moisture free air. The thickness of TiO₂ electrodes and the deposited scattering layers was determined using Dekker Profilometer. Surface morphology of the screen-printed TiO₂ nanoparticles was observed using EVOI MA10 (ZEISS) multipurpose scanning electron microscope operating at 20 kV employing secondary electron signals while the corresponding Energy Dispersive Spectra (EDS) were obtained using characteristic x-rays emitted by TiO₂ nanoparticles. The

X-ray diffraction (XRD) pattern of the screen-printed TiO₂ nanoparticles at room temperature was recorded using X-ray Diffractometer; Panalytical Xpert-Pro, PW3050/60, operating at 30 mA and 40 kV, with monochromatic *Cu-K α* radiation, of wavelength $\lambda = 1.54060 \text{ \AA}$. A scanned range $3\text{--}80.00553^\circ 2\theta$, with a step width of 0.001° was used. The pattern was analyzed and the peaks were identified using *ICDD* data file (*01-075-8897*). The UV-Visible (*UV-Vis*) absorption measurements of the dye extract and the dye extract on the screen printed TiO₂ electrodes were carried out with Avante UV-VIS spectrophotometer (model-*LD80K*). From these measurements, plots for the absorbance, Light Harvesting Efficiency (LHE) and molar extinction coefficient versus the wavelengths of interest were obtained using the relevant expressions from [16]. Few drops each of aniline and K₂Cr₂O₇ were coated on graphite foam by gently turning the graphite foam by hand to fabricate alternative counter electrode. The mixture was grown directly on graphite foam to preserve the stoichiometry. After the process, a greenish thin film of polyaniline (PANI) was formed atop the graphite foam signifying that there was no over oxidation of the aniline which would have reduced the conductivity. After drying, the surface of the counter electrode was thereafter rinsed using vitriol (H₂SO₄). Subsequently, the electrical characteristics of the semiconducting PANI deposited on soda lime glass following the above process were determined using ECOPIA HALL EFFECT MEASUREMENT SYSTEM (HMS-3000 VERSION 3.52). A DSC of 0.52 cm² active area was assembled by sandwiching a surlyn polymer foil of 25- μm thickness as spacer between the photoelectrode and the platinum counter electrode and then hot-pressed at 80 °C for 15s. A few drops of electrolyte were introduced into the cell assembly via a pre-drilled hole on the counter-electrode and sealed using amosil sealant. In order to have good electrical contacts, a strip of wire was attached to both sides of the FTO electrodes. Similarly, in assembling the modified DSC, the same process as above was adopted but instead of platinum counter electrode PANI coated on circular graphite foam was clamped onto the photoelectrode to form a monolithic cell of 0.78 cm² active area. Finally, the DSCs were subjected to current-voltage characterization using a standard overhead Veeco viewpoint solar simulator equipped with Air Mass 1.5 (AM 1.5) filter to give a solar radiation of 1000 W/m² and coupled to a source meter (Keithley, 4200SCS) which was connected to the computer via *GPIB* interface for data acquisition. Subsequently, the working electrode and counter electrode of the DSC were connected in turn to the positive and negative terminals of the digital *Keithley* source meter respectively. The bias was from short circuit to open circuit and was obtained automatically using LabVIEW software from National Instruments Inc, USA. From the data, *I-V* curves were plotted in real time for the DSCs under illuminated condition. Following this, the photovoltaic parameters viz; the open circuit voltage (V_{oc}) and short circuit current (I_{sc}) were obtained from the *I-V* curves for the cells. The fill factor (*FF*) and the power conversion efficiency were also calculated for the cells.

3. Results and Discussion

The thicknesses of the deposited TiO₂ and scattering layers on the FTO conducting glass were determined using Dekker Profilometer to be 5.2 μm and 1 μm respectively for the DSCs with unmodified photoelectrodes. The surface profiles from Dekker Profilometer for the deposited rGO and PANI are given in figure 1 for the DSC with modified electrodes. The thicknesses of the deposited rGO-TiO₂ layer and that of the deposited PANI on the soda lime glass were determined to be 4 μm and 46 nm respectively.

The images presented in figure 2 obtained using back scattered secondary electrons for TiO₂ nanoparticles was observed at a magnification of 83.04 kX while that for rGO-TiO₂ was

at 1.5 kX and that for PANI was at 0.35 kX. The uniform contrast in the image presented in figure 2(a) revealed TiO₂ to be practically isomorphic and the morphology of TiO₂ nanoparticles is such that the particles are closely parked and spherical in shape. The average diameter of the particles is in the range of 25-40 nm reflecting that TiO₂ nanoparticles are transparent and suitable for DSC application. The contrast variation in the image presented in figure 2(b) revealed the existence of TiO₂ and rGO phases with TiO₂ as the host matrix appearing in light contrast while rGO nanosheets are interspersed over the host matrix in dark contrast. The uniform contrast in the image presented in figure 2(c) revealed PANI to be isomorphic and the morphology of PANI is such that the microcrystalline domains are short range with numerous discontinuities appearing as void spaces in dark contrast. The XRD pattern shown in fig. 2(d) revealed the compound name for the TiO₂ electrode to be anatase syn., and the structure type is tetragonal with lattice constants $a = 3.7927 \text{ \AA}$ and $c = 9.5091 \text{ \AA}$. The most prominent peak has a d -spacing of 3.53217 \AA at $2\theta = 25.2139^\circ$ (ICDD data file: 01-075-8897). Other prominent peaks occur at $2\theta = 37.7883^\circ, 48.0463^\circ, 53.9110^\circ, 55.0481^\circ, 62.7104^\circ$ and 75.1376° with d -spacing $d = 2.38075 \text{ \AA}, 1.89370 \text{ \AA}, 1.70073 \text{ \AA}, 1.66826 \text{ \AA}, 1.48160 \text{ \AA}$ and 1.26338 \AA .

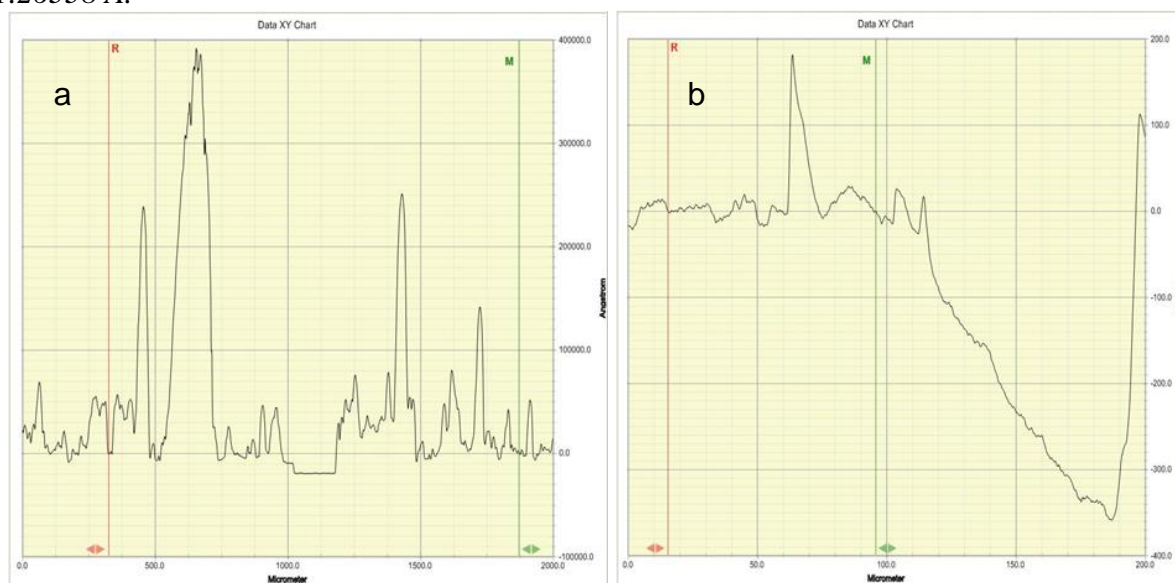


Figure 1. Surface profiles obtained using Dekker Profilometer for (a) rGO-TiO₂ and (b) PANI.

In figure 3, the dye extract exhibits absorption maximum slightly above 400nm and the most prominent shoulder occur slightly above 500nm. But upon sensitization on TiO₂ and rGO-TiO₂, there was a decrease in the absorption maxima and shoulder with a cut off slightly above 600nm. In our study, a shift in the absorption maximum towards higher energy of the spectrum was observed for the dye extracts adsorbed on rGO-TiO₂ nanocomposite with an improvement in the higher wavelengths up to 1000 nm. This observation suggests that there was weak adsorption of the dye extract onto surface of rGO-TiO₂ nanocomposite which could be attributed to the high pH value and the long bond length of the OH groups present in the dye extract. The shift may also be attributed to the changing of the anthocyanin molecules from the more stable flavilium states to the unstable quinoidal states upon chelation [15]. In this work, we have also used TiO₂ thin film of thickness 5.2μm and the light harvesting efficiencies (LHE) of the dye extract adsorbed onto rGO- TiO₂ surface are close to unity.

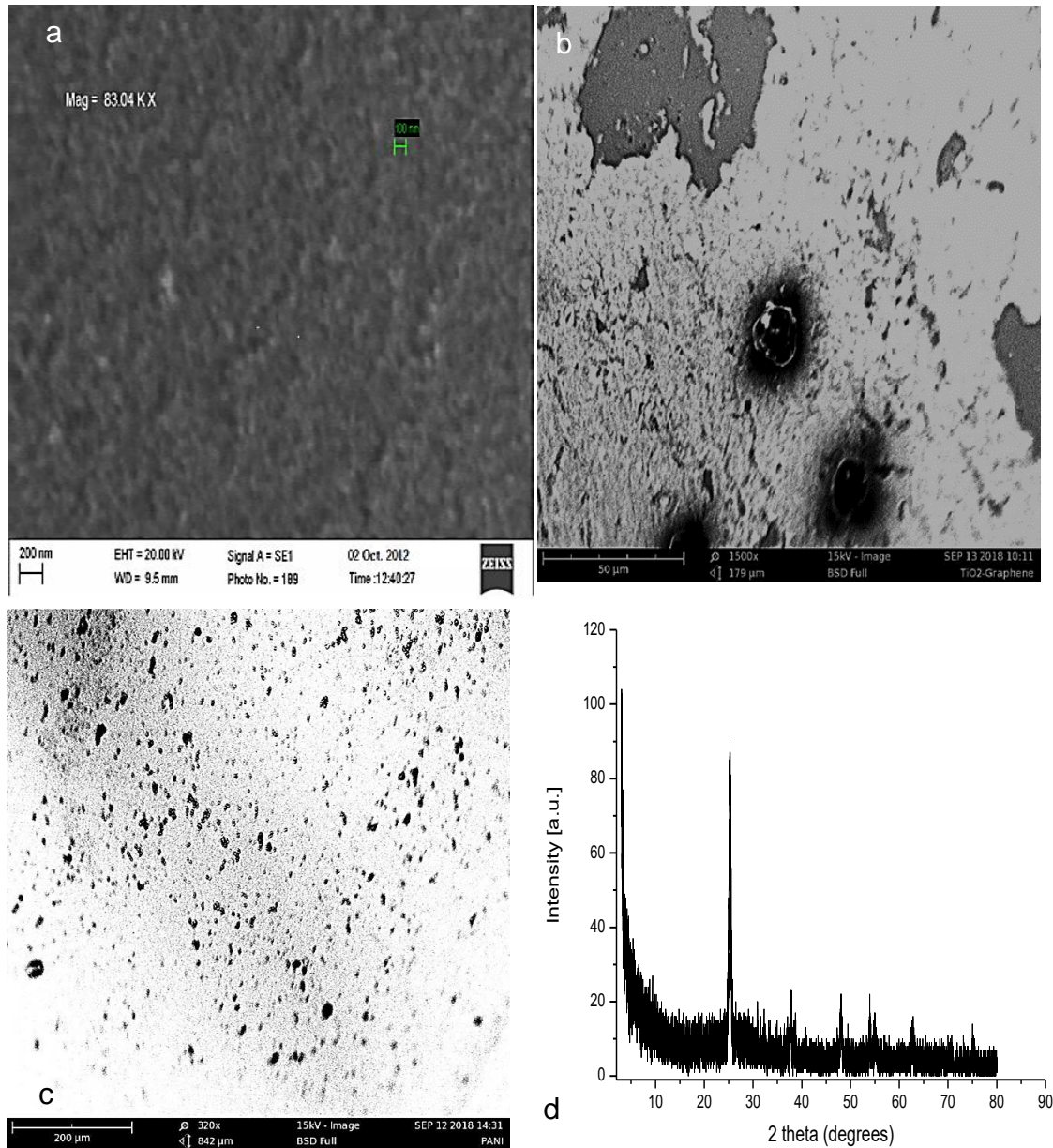


Figure 2. Microstructural characteristics: (a) TiO₂ photoelectrode (b) rGO-TiO₂ photoelectrode (c) PANI counter electrode and (d) XRD pattern for the screen printed TiO₂.

The electrical characteristics for PANI determined using ECOPIA HMS-3000 (VER 3.52) are tabulated in Table 1. It is evident from table 1 that the polymeric counter electrode (PANI) is semiconducting and it is a p-type semiconducting polymer with low mobility and conductivity values. The sign and the value of the Hall coefficient also validate the nature of the carrier. The bulk carrier concentration is $3.029 \times 10^{17} \text{ cm}^{-3}$. The IV and the IR characteristics are plotted in figures 4 (a) and (b). It is evident from the IV characteristics for PANI (figure 4a) that there exists a transition between the two linear regions of the curve at 0.3 Volts. The linear behaviour of PANI is seen above and below this region of transition, thus as synthesized PANI is ohmic for most part of the curve. This also shows that the as-synthesized PANI has non-ohmic character for this short region of transition and this is clearly revealed in the IR curves. Thus, this behaviour exhibited by PANI can be exploited for

the fabrication of rectifiers and photodiodes. (The sentence highlighted in red should be deleted)

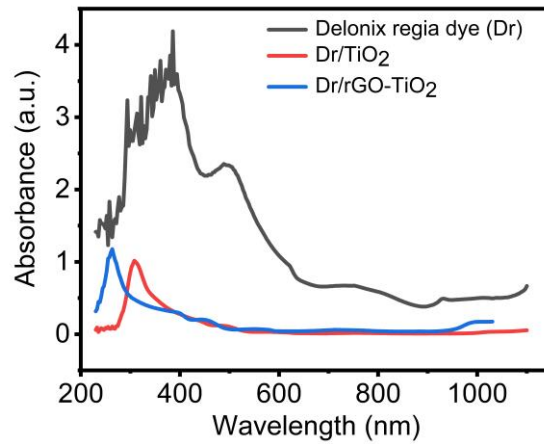


Figure 3. Absorption spectra for Delonix regia (Dr) dye extract, Dr/TiO and Dr/rGO-TiO₂.

Current density and power versus voltage characteristics for the DSCs are plotted and shown in figure 5. The photovoltaic parameters are determined and tabulated in Table 2. The current density for the rGO-TiO₂ DSC with PANI counter electrode is 0.45 mAcm⁻² while that for the unmodified TiO₂ DSC with PANI counter electrode is 0.11 mAcm⁻².

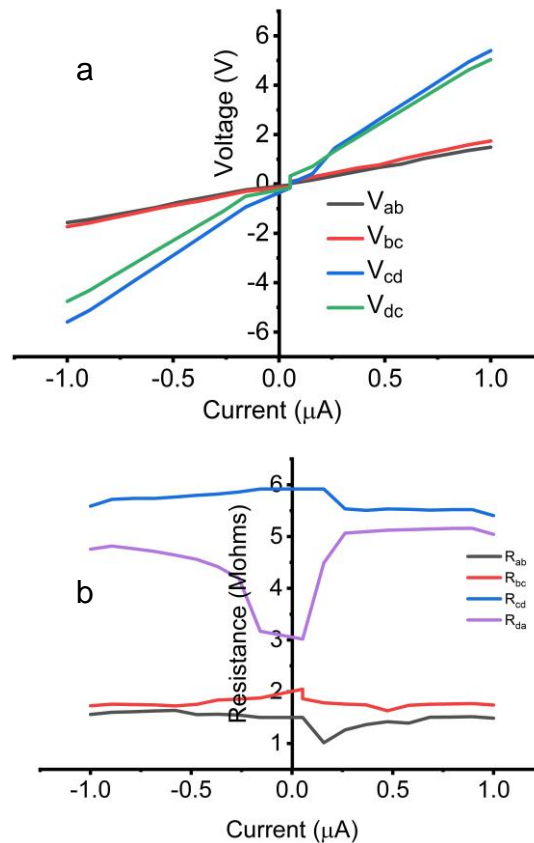


Figure 4. (a) IV and (b) IR Characteristics for PANI.

Table 1. Electrical Characteristics of PANI.

Bulk Concentration	$3.029 \times 10^{17} \text{ cm}^{-3}$
Mobility	$1.009 \times 10^1 \text{ cm}^2\text{V}^{-1}\text{s}^{-1}$
Resistivity	$2.043 \text{ } \Omega \text{ cm}$
Magneto resistance	$9.451 \times 10^4 \text{ } \Omega$
Conductivity	$4.894 \times 10^{-1} \text{ } \Omega^{-1} \text{ cm}^{-1}$
Hall coefficient	$2.061 \times 10^1 \text{ cm}^3\text{C}^{-1}$
Sheet resistance	$6.50 \times 10^5 \text{ } \Omega$

Table 2. Photovoltaic Parameters of DSCs sensitized with Delonix regia dye.

DSC	J_{sc} (mA/cm²)	V_{oc} (V)	FF	η (%)
Monolithic rGO-TiO₂ DSC with PANI electrode	0.45	0.47	0.60	0.13
Monolithic TiO₂ DSC with PANI electrode	0.11	0.56	0.60	0.04
Movable TiO₂ DSC with Platinum electrode	0.10	0.45	0.38	0.02

This corresponds to 76% increase in the current density and this drastically reduced electron recombination rate and increases collection rate at the photoelectrode. In the same light, a 16% decrease in the open circuit voltage (V_{oc}) was observed for the rGO-TiO₂ DSC with PANI counter electrode. Thus, the addition of rGO to TiO₂ led to a decrease in the difference between the Fermi levels of the modified TiO₂ photoelectrode and the redox potential of the redox electrolyte. The DSC assembled with the rGO-TiO₂ nanocomposite photoelectrode and PANI as counter electrode demonstrated an enhanced power conversion efficiency of 0.13% compared with 0.04% and 0.02% for the DSCs assembled with unmodified TiO₂ with PANI and platinum as counter electrode, respectively. This represents approximately 69% enhancement of power conversion efficiency in the DSC consisting of TiO₂ modified with rGO compared to that of DSC based on bare TiO₂ DSC with PANI electrode and roughly 85% increase in the power conversion efficiency over the bare TiO₂ DSC with platinum electrode. Thus, it is evident from table 2 that high values of J_{sc} , and V_{oc} are responsible for the higher power conversion efficiency. Nevertheless, the rGO-TiO₂-DSC//Delonix regia dye//PANI electrode proved to be a better cell compared to TiO₂-DSC//Delonix regia dye//PANI electrode and TiO₂-DSC//Delonix regia dye//Platinum electrode that exhibited lower power conversion efficiency. However, no deviation from this

trend was observed when the duration of continuous stimulated sunlight illumination was increased for several hours.

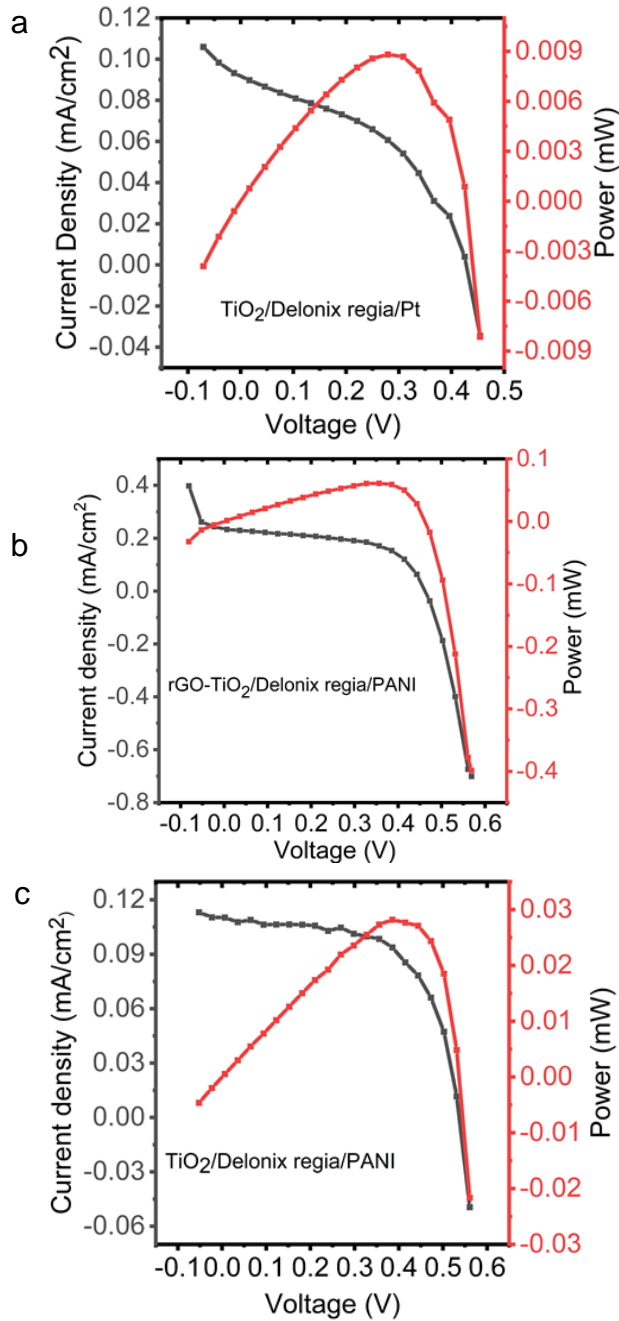


Figure 5. Current density and Power versus voltage for (a) unmodified TiO_2 DSC//Delonix regia dye//Platinum electrode, (b) unmodified TiO_2 DSC//Delonix regia dye//PANI electrode and (c) rGO-TiO_2 DSC//Delonix regia dye//PANI electrode.

4. CONCLUSION

In this work we have reported an investigation on Delonix regia dye extract as a natural sensitizer for rGO-TiO_2 -DSC//Delonix regia dye//PANI electrode, TiO_2 -DSC//Delonix regia dye//PANI electrode and TiO_2 -DSC//Delonix regia dye//platinum electrode. After the addition

of rGO to TiO₂ photoelectrode, the modified photoelectrode displayed enhanced dye adsorption properties with lower internal resistances, faster electron transport and lower charge recombination rate, which resulted in a high current density. The short circuit current density for the rGO-TiO₂ DSC with PANI counter electrode is 0.45 mAcm⁻² while that for the unmodified TiO₂ DSCs with PANI counter electrode and platinum counter electrode are 0.11 mAcm⁻² and 0.10 mAcm⁻² respectively. This corresponds to 76% increase in the current density and increases collection rate at the photoelectrode leading to enhanced power conversion efficiency of 0.13% compared with 0.04% and 0.02% for the DSCs assembled with unmodified TiO₂. This represent 69% enhancement of energy conversion efficiency in the DSC consisting of rGO modified TiO₂ compared with the results obtained in our previous work [40]. In view of this, we have explored the use of modified TiO₂, an alternative counter electrode and Delonix regia dye extract and this led to enhanced power-conversion efficiency of the DSC based on rGO-TiO₂ using PANI as counter electrode with Delonix regia as photosensitizer

ACKNOWLEDGMENT

We thank Physics Advanced Laboratory, Sheda Science and Technology Complex, Abuja, Nigeria for technical assistance during the experimental characterization.

REFERENCES

- [1] J. Li, A. C. Grimsdale, Carbazole-based Polymer for Organic photovoltaic devices, Chemical Society Reviews, 39 (2010) 2399-2410. <https://doi.org/10.1039/B915995A>
- [2] U. Bach, D. Lupo, P. Comte, J. E. Moser, F. Wiessortel, J. Salbeck, H. Spreitzer, M. Gratzel, Solid-State Dye-Sensitized Mesoporous TiO₂ Solar Cells with High Photon-to-Electron Conversion Efficiencies, Nature, 395 (1998) 583-585. <https://doi.org/10.1038/26936>
- [3] A. Yella, H. Lee, H.N. Tsao, C. Yi, A. K. Chandiran, M. K. Nazeerudin, E. W. Diau, C. Yeh, S. M. Zakeeruddin, M. Gratzel, Porphyrin-Sensitized Solar Cells with Cobalt (II/III)-Based Redox Electrolyte Exceed 12% Efficiency, Science, 334 (2011) 629-634. <https://doi.org/10.1126/science.1209688>
- [4] A. Hagfeldt, S.E. Lindquist, M. Gratzel., Charge carrier separation and charge transport in nanocrystalline junctions, Sol. Energy Mater. Sol. Cells, 32 (1996) 245-257. [https://doi.org/10.1016/0927-0248\(94\)90262-3](https://doi.org/10.1016/0927-0248(94)90262-3)
- [5] L. Kavan, M. Gratzel, S. E. Gilbert, C. Klemenz, H. J. Scheel, Electrochemical and photoelectrochemical investigation of single crystal anatase, J. Am. Chem. Soc., 118 (1996) 6716-6723. <https://doi.org/10.1021/ja954172l>
- [6] J. Bisquert, G. Garcia-Belmonte, F.J. Fabregat-Santiago, Modeling the electric potential distribution in the dark in nanoporous semiconductor electrodes, Solid State Electrochem., 3 (1999) 337-347. <https://doi.org/10.1007/s100080050164>
- [7] Y. Tachibana, J. E. Moser, M. Gratzel, D. Klug, J.R. Durrant, Subpicosecond interfacial charge separation in dye-sensitized nanocrystalline titanium dioxide films, J. Phys. Chem., 100 (1996), 20056-20062. <https://doi.org/10.1021/jp962227f>
- [8] A. Kay, M. Gratzel, Dye-sensitized core shell nanocrystals: Improved efficiency of mesoporous tin oxide electrodes coated with a thin layer of an insulating oxide, Chem. Mater., 14 (2002) 2930-2935. <https://doi.org/10.1021/cm0115968>

- [9] G.G.A. Kumara, K. Tennakone, V.P.S. Perera, A. Konno, S. Kaneko, M. Okuya, Suppression of recombination in a dye-sensitized photoelectrochemical cell made from a film of tin IV oxide crystallites coated with a thin layer of aluminium oxide, *J. Phys. D Appl. Phys.*, 34 (2001) 868-873. <https://doi.org/10.1088/0022-3727/34/6/306>
- [10] K. Tennakone, J. Bandara, P.K.M. Bandaranayake, G.G.A. Kumara, A. Konno, Enhanced efficiency of a dye-sensitized solar cell made from MgO-coated nanocrystalline SnO₂, *Jpn. J. Appl. Phys.*, 40 (2001) L732. <https://doi.org/10.1143/jjap.40.L732>
- [11] K. Tennakone, V.P.S. Perera, I.R.M. Kottegoda, L.A.A. De Silva, G.G.A. Kumara, A. Konno, Dye-sensitized photovoltaic cells: Suppression of electron-hole recombination by deposition of the dye on a thin insulating film in contact with a semiconductor, *J. Electron. Mater.*, 30 (2001) 992-996. <https://doi.org/10.1007/bf02657723>
- [12] B.A. Gregg, F. Pichot, S. Ferrere, C.L. Fields., Interfacial recombination processes in dye-sensitized solar cells and methods to passivate the interfaces, *J. Phys. Chem. B*, 105 (2001) 1422-1429. <https://doi.org/10.1021/jp003000u>
- [13] R. Kennedy, I. Martini, G. Hartland, P.V. Kamat., Capped semiconductor colloids: Synthesis and photochemistry of CdS capped SnO₂ nanocrystallites, *Proc. Indian Acad. Sci. Chem. Sci.*, 109 (1997) 497-507. <https://doi.org/10.1007/bf02869209>
- [14] C. Nasr, P.V. Kamat, S. Hotchandani., Photoelectrochemistry of composite semiconductor thin films: Photosensitization of SnO₂/CdS coupled nanocrystallites with a ruthenium polypyridyl complex, *J. Phys. Chem. B*, 102 (1998) 10047-10056. <https://doi.org/10.1021/jp970833k>
- [15] P.A. Sant, P. V. Kamat., Interparticle electron transfer between size-quantized CdS and TiO₂ semiconductor nanoclusters., *Phys. Chem. Chem. Phys.*, 4 (2002) 198-203. <https://doi.org/10.1039/b107544f>
- [16] I. Bedja, P.V. Kamat., Capped semiconductor colloids: Synthesis and photoelectrochemical behaviour of TiO₂ capped SnO₂ nanocrystallites., *J. Phys. Chem.*, 99 (1995) 9182-9188. <https://doi.org/10.1021/j100022a035>
- [17] S. Chappel, S.G. Chen, A. Zaban., TiO₂ coated nanoporous SnO₂ electrodes for dye-sensitized solar cells, *Langmuir*, 18 (2002) 3336-3342. <https://doi.org/10.1021/la015536s>
- [18] S.G. Chen, S. Chappel, Y. Diamant, A. Zaban., Preparation of Nb₂O₅ coated TiO₂ nanoporous electrode and their application in dye-sensitized solar cells, *Chem. Mater.*, 13 (2001) 4629-4634. <https://doi.org/10.1021/la051807d.s001>
- [19] G.G.A. Kumara, A. Konno, K. Tennakone., Photoelectrochemical cells made from SnO₂/ZnO films sensitized with Eosin dyes, *Chem. Lett.*, 12 (2001) 180-181. <https://doi.org/10.1246/cl.2001.180>
- [20] H. Tada, A. Hattori., A patterned TiO₂/SnO₂ bilayer type photocatalyst, *J. Phys. Chem. B*, 104 (2000) 4585-4604. <https://doi.org/10.1021/jp000049r>
- [21] K. Tennakone, G.K.R. Senadeera, V.P.S. Perera, I.R.M. Kottegoda, L.A.A. De Silva, Dye-sensitized photoelectrochemical cells based on porous SnO₂/ZnO composite TiO₂ films with a polymer electrolyte, *Chem. Mater.*, 11 (199) 2474-2477. <https://doi.org/10.1021/cm990165a>
- [22] A. Zaban, S.G. Chen, S. Chappel, B.A. Gregg, Bilayer nanoporous electrodes for dye-sensitized solar cells, *Chem. Commun*, 22 (2000) 2231-2232. <https://doi.org/10.1039/B005921H>
- [23] S. Burnside, J.E. Moser, K. Brooks, M. Gratzel, D. Cahen., Nanocrystalline mesoporous strontium titanate as photoelectrode materials for photosensitized solar devices: increasing photovoltage through flat band potential engineering, *J. Phys. Chem. B*, 103 (1999) 9328-9332. <https://doi.org/10.1021/jp9913867>
- [24] F. Lenzmann, J. Krueger, S. Burnside, K. Brooks, M. Gratzel, D. Gal, S. Ruhle, D. Cahen,

Surface photovoltage spectroscopy of dye-sensitized solar cells with TiO₂, Nb₂O₅ and SrTiO₃ nanocrystalline photoanode: an indication for electron injection from higher excited dye states, *J. Phys. Chem. B*, 105 (2001) 6347-6352. <https://doi.org/10.1021/jp010380q>

[25] Y. Diamant, S. G. Chen, O. Melamed, A. Zaban., Core-Shell Nanoporous Electrode for Dye Sensitized Solar Cells: The Effect of the SrTiO₃ Shell on the Electronic Properties of the TiO₂ Core, *J. Phys. Chem. B*, 107 (2003) 1977-1981. <https://doi.org/10.1021/jp027827v>

[26] A.K. Geim, K.S. Novoselov, The rise of graphene, *Nat. Mater*, 6 (2007) 183–191. <https://doi.org/10.1038/nnano.2010.224>

[27] Q.J. Xiang, J.G. Yu, M. Jaroniec, Graphene-based semiconductor photocatalysts, *Chem. Soc. Rev*, 41 (2012) 782–796. <https://doi.org/10.1039/C1CS15172J>

[28] R.K.Yadav, J.O. Baeg, G.H. Oh, N.J. Park, K.J. Kong, J. Kim, D.W. Hwang, S.K. Biswas., A photocatalyst-enzyme coupled artificial photosynthesis system for solar energy in production of formic acid from CO₂, *J. Am. Chem. Soc*, 134 (2012) 11455–11461. <https://doi.org/10.1021/ja3009902>

[29] W.S. Hummers, R.E. Offeman, Preparation of graphitic oxide, *J. Am. Chem. Soc.*, 80 (1958) 1339. <https://doi.org/10.1021/ja01539a017>

[30] X.F. Gao, J. Jang, S. Nagase., Hydrazine and thermal reduction of graphene oxide: Reaction mechanisms, product structures, and reaction design, *J. Phys. Chem. C.*, 14 (2010) 832–842. <https://doi.org/10.1021/jp909284g>

[31] S.D. Perera, R.G. Mariano, N. Nijem, Y. Chabal, J.P. Ferraris, K.J. Balkus., Alkaline deoxygenated graphene oxide for supercapacitor applications: An effective green alternative for chemically reduced graphene, *J. Power Sources.*, 215 (2012) 1–10. <https://doi.org/10.1016/j.jpowsour.2012.04.059>

[32] T. Soltani, B.K. Lee., Sono-synthesis of nanocrystallized BiFeO₃/reduced graphene oxide composites for visible photocatalytic degradation improvement of bisphenol., *A. Chem. Eng. J.*, 306 (2016) 204–213. <https://doi.org/10.1016/j.cej.2016.07.051>

[33] M. Debabrata, A. Chayan, K.G. Barun, C. Madhurya, N.G. Narendra., One-Dimensional BiFeO₃ nanowire-reduced graphene oxide nanocomposite as excellent supercapacitor electrode material, *ACS Appl, Energy Mater.*, 1 (2018) 464–474. <https://doi.org/10.1021/acsam.7b00097.s001>

[34] Q. Zhao, R.F. Liu, Y.L. Shen, M.L. Fang, M.F. Dong., Highly efficient visible-light-driven graphene-CdS nanocomposite photocatalysts, *J. Nanosci. Nanotechnol*, 18 (2018) 4755–4763. <https://doi.org/10.1166/jnn.2018.15344>

[35] D.F. Xu, L.L. Li, R.A. He, L.F. Qi, L.Y. Zhang, B. Cheng., Noble metal-free RGO/TiO₂ composite nanofiber with enhanced photocatalytic H₂-production performance, *Appl. Surf. Sci.*, 434 (2018) 620–625. <https://doi.org/10.1016/j.apsusc.2017.10.192>

[36] F. Hosseini, S. Mohebbi, Photocatalytic oxidation based on modified titanium dioxide with reduced graphene oxide and CdSe/CdS as nanohybrid materials, *J. Clust. Sci.*, 29 (2018) 289–300. <https://doi.org/10.1007/s10876-017-1326-6>

[37] B. J. Liu, L. Lin, D. Yu, J. Sun, Z.J. Zhu, P. Gao, W. Wang, Construction of fiber-based BiVO₄/SiO₂/reduced graphene oxide (RGO) with efficient visible light photocatalytic activity, *Cellulose*, 25 (2018) 1089–1101. <https://doi.org/10.1007/s10570-017-1628-8>

[38] S. P. Lim, A. Pandikumar, N.M. Huang, H.N. Lim, Reduced graphene oxide–titania nanocomposite-modified photoanode for efficient dye-sensitized solar cells., *Int. J. Energy Res.*, 39 (2015) 812-824. <https://doi.org/10.1002/er.3307>

[39] L. Wei, S. Chen, Y. Yang, Y. Dong, W. Song, R. Fan, Reduced graphene oxide modified TiO₂ semiconductor materials for dye-sensitized solar cells, *RSC Advances*, 6 (2016) 100866-100875. <https://doi.org/10.1039/C6RA22112B>

[40] T. O. Ahmed, N. Alu, A. Y. AbdulRahman., Comparative Study on the Photovoltaic Properties of Dye-Sensitized Solar Cells (DSCs) Based on Different Counter Electrode Configurations, Journal of Materials Science Research and Reviews, 3 (2019) 1-9.
<https://journaljmsrr.com/index.php/JMSRR/article/view/30088>